ELECTRICAL IMPEDANCE TOMOGRAPHY FOR DAMAGE DETECTION AND LOCALIZATION ON CARBON FIBRE REINFORCED POLYMER COMPOSITES

Helena, Rocha[a, b], Christophe, Fernandes[c], Nelson, Ferreira[c], Ugo, Lafont[d], João P., Nunes[a]

a: Institute for Polymers and Composites, University of Minho, Guimarães, Portugal – helenarocha@dep.uminho.pt
b: PIEP – Innovation in Polymer Engineering, Guimarães, Portugal
c: Stratosphere, Guimarães, Portugal
d: European Space Agency, Noordwijk, The Netherlands

Abstract: *Electrical impedance tomography (EIT) is being developed as promising non-intrusive technology for damage detection in conductive fibre reinforced polymers (FRP) composites. This work assessed EIT and one-step difference Gaussian-Newton algorithm to detect different damages in CFRP laminates, including through-thickness holes and impact damage of different severities. Two layup laminates were studied: quasi-isotropic [0/45/90/-45]s and unbalanced [0/0/45/90/-45]s. Each laminate configuration was subjected to three levels of impact energy. Through-thickness holes with diameters as small as 2 mm were detected. The LVI on unbalanced specimens created elongated shaped damages, which were observed through EIT and ultrasonic C-scan. Differently, the ultrasonic C-scan inspections revealed circular shaped damages on the centre of the quasi-isotropic specimens, while EIT could not reveal a well-defined damage shape. Yet, the presence of damage was observed in the centre of the specimens by EIT. Although EIT overestimated the damaged area, it was highly sensitive to the imposed damages.*

Keywords: Carbon Fibre Reinforced Polymer Composite; Electrical Impedance Tomography; Impact Damage Detection; Barely Visible Impact Damage; Through-thickness hole

1. Introduction

The performance of FRP composites is particularly affected by the presence of barely visible impact damage, produced by low velocity impacts (LVI) (1). Several approaches for impact damage detection and localization on composites are addressed in the literature. Although various types of sensors have been already embedded in composite structures for damage detection, like optical fibre-based and piezoelectric ones, their presence may affect the mechanical performance of such structures (2). Alternatively, as electrical impedance tomography (EIT) technique uses surface electrodes instead of invasive sensors, their use does not affect the performance of composites (3). Electrodes are mounted on the boundary of an electrically conductive composite, such as carbon fibre reinforced polymer (CFRP) composites or composites with conductive particles modified matrices (4–7). Current is injected though a pair of electrodes, and resultant voltages in the following pairs are measured (3). This allows to construct tomographic images of the distribution of spatial electrical conductivity. Despite the reduced spatial resolution, EIT can detect subtle conductivity variations when damages like cracks or delaminations disrupt the conductive network (8). Yet, the EIT technology remains at low TRL regarding monitoring of anisotropic materials such as composites, in contrast to conductive anisotropic materials like metals.

  doi:10.5075/epfl-298799_978-2-9701614-0-0

Algorithms for reconstruction of static electrical impedance tomography images may lead to measurement errors, due to the higher sensitivity of EIT to changes in the boundary proximity than within the sample. A slight error on electrode positioning may generate similar voltage measurements to those of a severe inhomogeneity in the middle of a specimen. Alternatively, algorithms for dynamic imaging reconstruction avoid this limitation of static EIT. In dynamic EIT reconstruction, the conductivity image at time instant t_2 is determined by the difference of voltage v_2, at t_2, and of the prior measured voltage v_1 at time instant t_1 (9). Thus, the EIT voltage difference, *y*, can be calculated resorting to Eq. (1) (10).

$$[y]_i = [v_2]_i - [v_1]_i \tag{1}$$

The medium conductivity is modelled using a finite element model, comprising n_N elements, which are represented by the vector of conductivity $\sigma \in \mathbb{R}^{n_N}$. The difference EIT can also be obtained through the conductivity change vector, *x,* given by the difference of conductivity distribution σ_2, at t_2, and the conductivity distribution σ_1, at t_1, as stated in Eq. 2 (10).

$$x = \sigma_2 - \sigma_1 \tag{2}$$

To obtain the boundary voltage data from the measured reference conductivity, and solve the forward problem in the difference EIT methodology, the linear Eq. 3 is applied (10).

$$y = Jx + n \tag{3}$$

being *J* the Jacobian matrix and *n* the measurement noise.

This work used a one-step difference Gaussian-Newton (GN) algorithm to solve the inverse problem of EIT and to construct the EIT images. The conductivity can be promptly calculated as a linear matrix, facilitating real-time EIT image reconstruction. The one-step GN algorithm searches for the minimized solution $\hat{x}$, given by the minimized sum of quadratic norms, as presented in Eq. 4 (10).

$$\|y - J\hat{x}\|^2_{\sum n^{-1}} + \|x - x^0\|^2_{\sum x^{-1}} \tag{4}$$

where x^0 is the anticipated conductivity changes in the element, being null for difference EIT, $\sum_n$ is the covariance matrix of *n* and $\sum_x$ is the projected image covariance.

A one-step linearized inverse solution is given in Eq. 5 (10).

$$\hat{x} = (J^T W J + \lambda^2 R)^{-1} J^T W y \tag{5}$$

being *W* and *R* heuristically calculated, as presented in Eq. 6 and 7, respectively, *R* the regularization matrix, and λ the hyperparameter, calculated through Eq. 8.

$$W = \sigma_n^2 \sum n^{-1} \tag{6}$$

$$R = \sigma_x^2 \sum x^{-1} \tag{7}$$

$$\lambda = \frac{\sigma_n}{\sigma_x} \tag{8}$$

where σ_n is the average amplitude of *n* and σ_x is the initial conductivity change.

This work explored EIT technique with one-step difference GN algorithm to detect different damages in CFRP laminates, namely through-thickness holes, and impact damage of different

  doi:10.5075/epfl-298799_978-2-9701614-0-0

severities. Two layup configurations were produced and evaluated: a quasi-isotropic configuration, believed to present a more isotropic-like behaviour and an unbalanced configuration, believed to present a more anisotropic-like behaviour. Each laminate configuration was subjected to three levels of impact energy drilled with fully through-thickness holes. Ultrasonic C-scan inspections were undertaken for comparison and validation of EIT.

2. Materials and Experimental Techniques

2.1. CFRP Laminates

CFRP laminates were made of epoxy, composed of Biresin® CR83 resin and CH83-6 hardener (Sika AG, Switzerland) mixed in a proportion of 100/30 wt%, respectively, and unidirectional carbon fibre fabric, 350UT (Toray Industries, Inc., Japan), with an areal weight of 340 g/m2. The laminates were produced with two different layup configurations: a quasi-isotropic laminate with 8 layers, [0/45/90/ 45]s, and an unbalanced laminate with 10 layers, [0/0/45/90/ 45]s.

The CFRP plates, measuring about 500 mm x 700 mm, were manufactured by vacuum assisted resin infusion (VARI). The laminates were initially left to cure at room temperature, under vacuum, for approximately 40 hours and then, post cured at 70 °C for around 8 hours at ambient pressure. The cured composite plates were cut into specimens of approximately 150 x 100 mm, according to ASTM D7136 standard, for impact testing.

2.3. Production of damage in the CFRP plates

Through-thickness holes were drilled on the CFRP specimens. The locations of the two through-thickness holes are represented by the red dots A and B in Figure 1. Hole A was firstly created having an initial 2 mm diameter, being later expanded to 4.5 and 6 mm. With hole A having a 6 mm diameter, hole B was then drilled following the same diameter increments as hole A. EIT imaging was recorded between each drilling step for diameter increase.

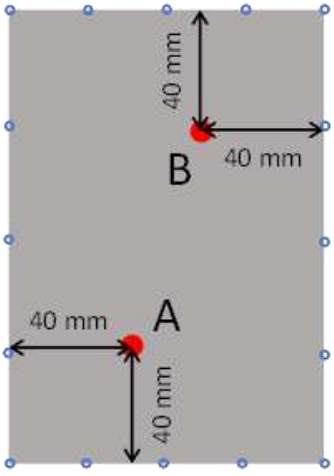

Figure 1. Red dots A and B indicate the location of the through-thickness holes

A drop-weight impact testing setup was used to produce impact damages. Distinct degrees of damage severity (unnoticed damage, barely visible damage, and severe damage) were enforced in the laminates. Different impact energies had to be employed on the distinct laminates to generate damages of equivalent severity, since the different layup configurations result in distinctive impact resistance. The quasi-isotropic and the unbalanced specimens were exposed

to impact energies of 20.0, 30.0 and 49.5 J and 15.0, 30.0 and 49.5 J, respectively. Each condition was replicated in three specimens. Drop-weight impact testing was conducted on the Fractovis Plus equipment from CEAST, with a 20 mm diameter hemispheric head impactor, with a mass of 5.045 kg. The vertical position of the impactor was adjusted between 305 and 1000 mm, producing the different levels of impact energy. Tests were conducted according to ASTM D7136 standard.

2.4. Damage Inspection

Each specimen, of 150 mm x 100 mm, had sixteen electrodes applied on its boundary for EIT analysis. The location of the electrodes is schematically represented by the blue circles in Figure 1 and it can be seen in Figure 2 (b) and (c). The EIT equipment, developed at Stratosphere company, comprised a power supply (XPH 35-4D Dual DC – Sorensen), a digital multimeter (2100 – Keithley) and a type-k thermocouple (see Figure 2 (a)). It was used the adjacent current injection method, where current is injected in one pair of adjacent electrodes and resultant voltages on all following adjacent electrodes pairs are measured. The inverse EIT problem was solved with one-step difference GN algorithm for image reconstruction. A λ of 1 was utilized for image reconstruction. Each specimen was analysed prior to damage creation to serve as reference baseline for EIT image reconstruction.

(a) (b) (c)

Figure 2. (a) EIT equipment; (b) specimens with 16 boundary electrodes being analysed and (c) detailed of a boundary electrode

Non-destructive ultrasonic C-scan inspections were performed on impacted specimens to provide a comparison and validate the EIT images. The ultrasonic C-scan inspections were carried out in an Omni Scan Sx – Olympus, using a 0.5 MHz M2008 probe. A two-axis encoder, with 1.0 mm and 3mm resolution in the axis along the specimens length and width, respectively, was used.

3. Results and discussion

Figure 3 and Figure 4 show the EIT reconstruction images of the quasi-isotropic and unbalanced specimen, respectively, with drilled holes A and B with progressive larger diameters. A decrease of electrical conductivity (darker blue) is observable in the bottom area of Figure 3 and Figure 4 (a), (b) and (c), showing larger and darker blue areas as the holes diameters are increased. Similarly, the production and diameter increase of hole B induced larger and darker blue areas in the top of Figure 3 and Figure 4 (d), (e) and (f). The created damages induced an electrical interference in the region close to the boundary electrodes. Nevertheless, the employed EIT method was sensitive to the presence of the smallest 2 mm diameter through-thickness hole.

  doi:10.5075/epfl-298799_978-2-9701614-0-0

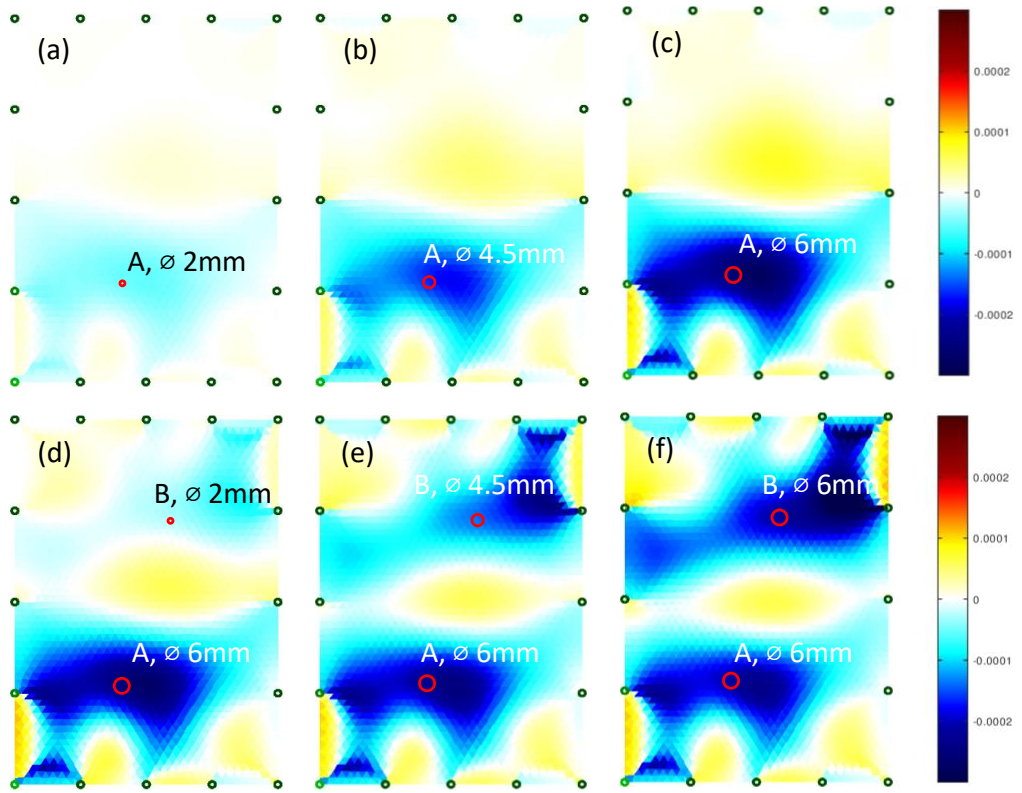

Figure 3. EIT images of a drilled quasi-isotropic specimen with through-thickness holes A and B having different diameters: (a) A: 2 mm, B: non-existent; (b) A: 4.5 mm, B: non-existent; (c) A: 6 mm, B: non-existent; (d) A: 6 mm, B: 2 mm; (e) A: 6 mm, B: 4.5 mm; (f) A: 6 mm, B: 6 mm. The green dots indicate the locations of the electrodes

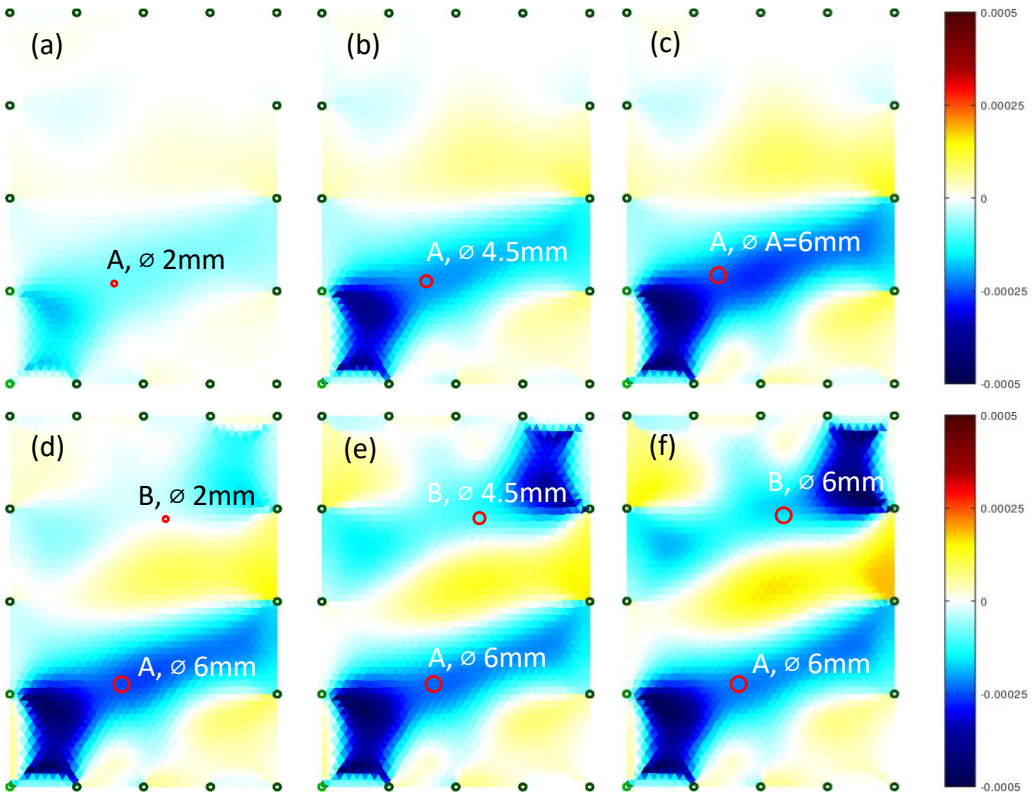

Figure 4. EIT images of a drilled unbalanced specimen with through-thickness holes A and B having different diameters: (a) A: 2 mm, B: non-existent; (b) A: 4.5 mm, B: non-existent; (c) A: 6 mm, B: non-existent; (d) A: 6 mm, B: 2 mm; (e) A: 6 mm, B: 4.5 mm; (f) A: 6 mm, B: 6 mm. The green dots indicate the locations of the electrodes

  doi:10.5075/epfl-298799_978-2-9701614-0-0

The impact events produced different damage shapes on the two laminates of different configuration. Contrary to the expectations, the quasi-isotropic specimens revealed an increase of electrical conductivity in the central region of the specimens, with undefined shape of damage (top of Figure 5). Contrarily, the unbalanced laminates (top of Figure 6) showed elongated "peanut" shaped damages (11), where a decrease of electrical conductivity can be seen. The ultrasonic inspections (bottom of Figure 5 and 6) verified the damage shapes created in the impacted laminates, where the EIT of unbalanced laminates overestimates the delamination areas in about 1.4 to 2 times.

It was expected that EIT would locate damage with improved accuracy in the quasi-isotropic laminate. Yet, the opposite was verified, which might be explained by the higher number of layers at 0°, yielding an improved path for electrical conduction in the unbalanced specimens.

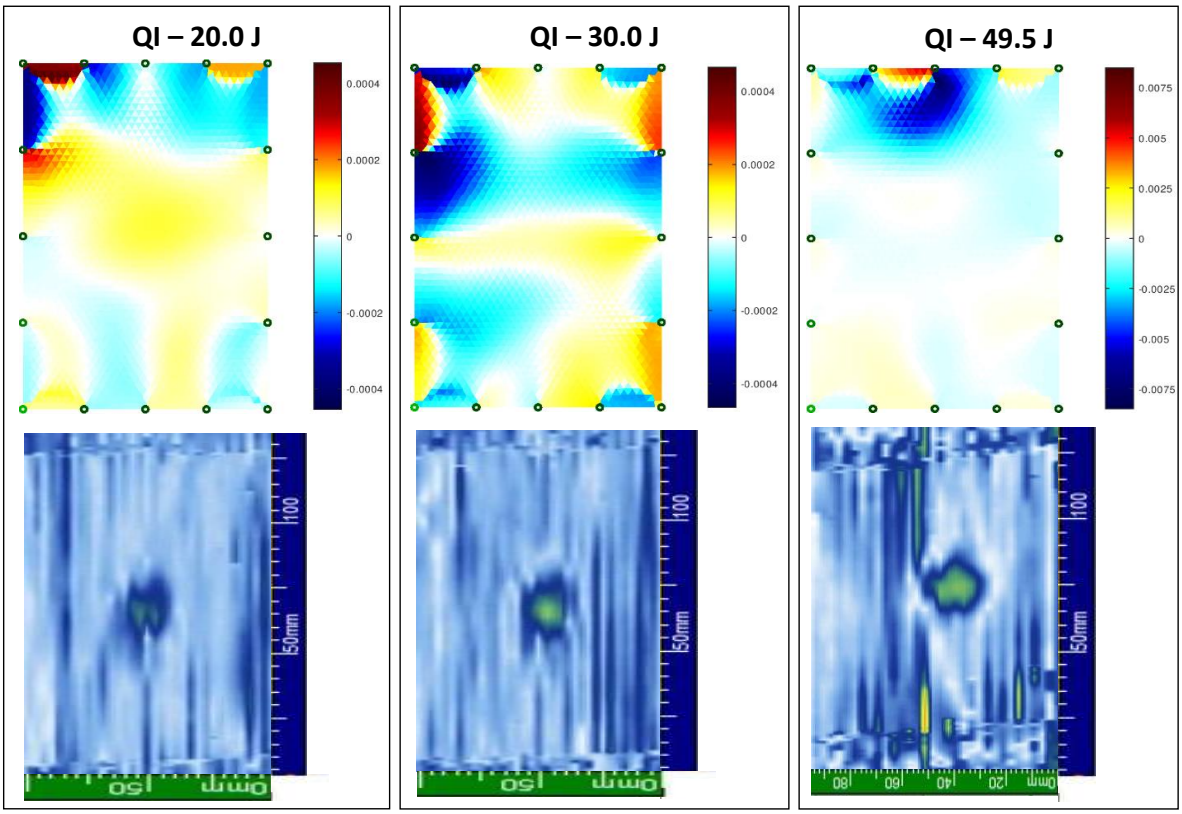

Figure 5. (top) EIT images and (bottom) ultrasonic C-scan inspection images of quasi-isotropic specimens damaged by Impacts of different energies: (left) 20.0J, (middle) 30.0 J, and (right) 49.5 J

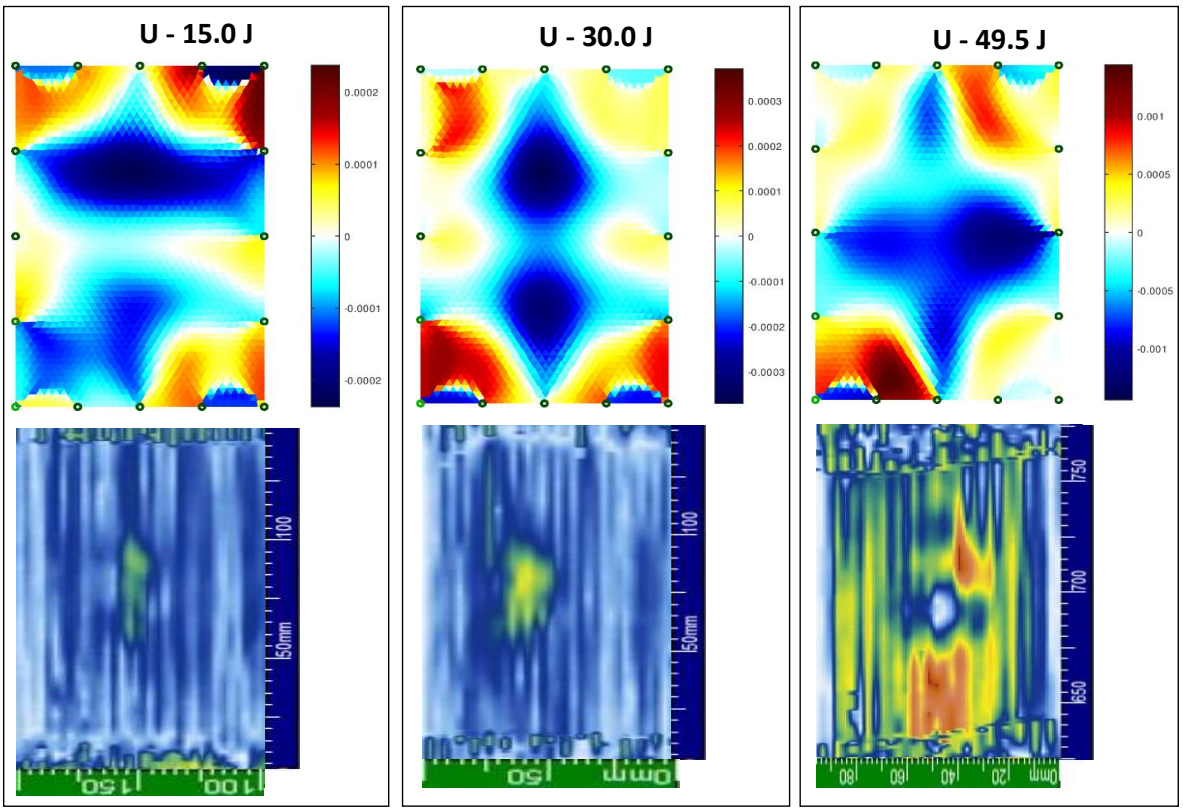

Figure 6. (top) EIT images and (bottom) ultrasonic C-scan inspection images of unbalanced specimens damaged by Impacts of different energies: (left) 15.0J, (middle) 30.0 J, and (right) 49.5 J

4. Conclusions

EIT with a one-step GN algorithm was evaluated for damage detection in CFRP composites. Different damage types were produced in the CFRP laminates: through-thickness holes and impact damage produced by impact testing with three levels of impact energy. CFRP plates with two distinct layup configurations (a quasi-isotropic and an unbalanced configuration) were manufactured by VARI process.

EIT was sensitive to through-thickness holes as little as 2 mm and showed progressively larger areas of decreased electrical conductivity, as the holes diameter increased.

The impacts on unbalanced specimens resulted on elongated shaped damages, “peanut” shape-like damage, which were observable by both EIT and ultrasonic C-scan inspections. The ultrasonic C-scan inspections revealed circular shaped damages in the impacted quasi-isotropic specimens, while the EIT images could not reveal a defined damage shape. Yet changes of electrical conductivity are visible in the specimens centre. Generally, the EIT technique overestimate the damaged area.

Acknowledgements

The authors would like to acknowledge the support of the European Regional Development Fund [grant number NORTE-01-0145-FEDER-000015]; and of the European Space Agency [Network/Partnering Initiative Program - ESA Contract 4000123315].

5. References

1. Giurgiutiu V. SHM of Aerospace Composites – Challenges and Opportunities. CAMX Conf Proc. 2015;1–15.

2. Ramakrishnan M, Rajan G, Semenova Y, Farrell G. Overview of Fiber Optic Sensor Technologies for Strain/Temperature Sensing Applications in Composite Materials. Sensors [Internet]. 2016;16(1):99. Available from: http://www.mdpi.com/1424-8220/16/1/99

3. Loyola BR, Saponara V La, Loh KJ, Briggs TM, Bryan GO, Skinner JL. Spatial Sensing Using Electrical Impedance Tomography. IEEE Sens J. 2013;13(6):2357–67.

4. Nonn S, Schagerl M, Zhao Y, Gschossmann S, Kralovec C. Application of electrical impedance tomography to an anisotropic carbon fiber-reinforced polymer composite laminate for damage localization. Compos Sci Technol [Internet]. 2018;160:231–6. Available from: https://doi.org/10.1016/j.compscitech.2018.03.031

5. Cagáň J, Pelant J, Kyncl M, Kadlec M, Michalcová L. Damage detection in carbon fiber–reinforced polymer composite via electrical resistance tomography with Gaussian anisotropic regularization. Struct Heal Monit. 2019;18(5–6).

6. Tallman TN, Gungor S, Wang KW, Bakis CE. Damage detection via electrical impedance tomography in glass fiber/epoxy laminates with carbon black filler. Struct Heal Monit. 2015;14(1):100–9.

7. Thomas AJ, Kim JJ, Tallman TN, Bakis CE. Damage detection in self-sensing composite tubes via electrical impedance tomography. Compos Part B Eng [Internet]. 2019;177(107276). Available from: https://doi.org/10.1016/j.compositesb.2019.107276

8. Cagáň J, Michalcová L. Impact Damage Detection in CFRP Composite via Electrical Resistance Tomography by Means of Statistical Processing. J Nondestruct Eval. 2020;39(2).

9. Adler A, Guardo R. Electrical impedance tomography: Regularized imaging and contrast detection. IEEE Trans Med Imaging. 1996;15(2):170–9.

10. Adler A, Dai T, Lionheart WRB. Temporal image reconstruction in electrical impedance tomography. Physiol Meas. 2007;28(7).

11. Abrate S. Impact on Composite Structures. Cambridge University Press; 1998.

